

# Morphological Studies of the SWIRE Galaxy Population in the UGC 10214 HST/ACS field

E. Hatziminaoglou<sup>1</sup>, P. Cassata<sup>2</sup>, G. Rodighiero<sup>2</sup>, I. Pérez-Fournon<sup>1</sup>,  
A. Franceschini<sup>2</sup>, A. Hernán-Caballero<sup>1</sup>, F.M. Montenegro-Montes<sup>1</sup>  
A. Afonso-Luis<sup>1</sup>, T. Jarrett<sup>3</sup>, G. Stacey<sup>4</sup>, C. Lonsdale<sup>5</sup>, F. Fang<sup>4</sup>, S. Oliver<sup>6</sup>,  
M. Rowan-Robinson<sup>7</sup>, D. Shupe<sup>3</sup>, H.E. Smith<sup>5</sup>, J. Surace<sup>3</sup>, C.K. Xu<sup>3</sup>,  
E.A. González-Solares<sup>8</sup>

<sup>1</sup>*Institute de Astrofísica de Canarias, C/ Via Lactea s/n, E-38200 La Laguna, Spain*

<sup>2</sup>*Dipartimento di Astronomia, Università di Padova, Vicolo Osservatorio 5, 35122 Padua, Italy*

<sup>3</sup>*Infrared Processing and Analysis Center, California Institute of Technology, Pasadena, CA 91125, USA*

<sup>4</sup>*Cornell University, Astronomy Department, Ithaca, NY 14853, USA*

<sup>5</sup>*Center for Astrophysics and Space Sciences, University of California, San Diego, La Jolla, CA 92093-0424, USA*

<sup>6</sup>*Astronomy Centre, Department of Physics and Astronomy, University of Sussex, Falmer, Brighton BN1 9QJ, UK*

<sup>7</sup>*Astrophysics Group, Blackett Laboratory, Imperial College London, London SW7 2BW, UK*

<sup>8</sup>*Institute of Astronomy, University of Cambridge, Madingley Road, Cambridge CB3 0HA, UK*

2 November 2018

## ABSTRACT

We present results of a morphological analysis of a small subset of the Spitzer Wide-area InfraRed Extragalactic survey (SWIRE) galaxy population. The analysis is based on public ACS data taken inside the SWIRE N1 field, which are the deepest optical high-resolution imaging available within the SWIRE fields as of today. Our reference sample includes 156 galaxies detected by both ACS and SWIRE. Among the various galaxy morphologies, we disentangle two main classes, spheroids (or bulge-dominated galaxies) and disk-dominated ones, for which we compute the number counts as a function of flux. We then limit our sample to objects with IRAC fluxes brighter than 10  $\mu$ Jy, estimated  $\sim 90\%$  completeness limit of the SWIRE catalogues, and compare the observed counts to model predictions. We find that the observed counts of the spheroidal population agree with the expectations of a hierarchical model while a monolithic scenario predicts steeper counts. Both scenarios, however, under-predict the number of late-type galaxies. These observations show that the large majority (close to 80 per cent) of the 3.6 and 4.5  $\mu$ m galaxy population, even at these moderately faint fluxes, is dominated by spiral and irregular galaxies or mergers.

**Key words:** galaxies: evolution – galaxies: elliptical and lenticular, cD – galaxies: spiral – galaxies: irregular – infrared: general – infrared: galaxies

## 1 INTRODUCTION

A key question on galaxy formation and evolution, in particular about the early-type sub-population which includes the most massive galaxies at any redshifts, is when and on which timescales their stellar content has been formed and assembled. Two schematic models are often confronted with the observations, the monolithic collapse model (Eggen et al. 1962; Larson 1975; Chiosi & Carraro 2002) and the hierarchical assembly scenario (e.g. White & Rees 1978; White & Frenk 1991; Somerville & Primack 1999;

Cole et al. 2000). In the monolithic collapse, a burst of star formation happened at very high redshifts ( $z_{\text{form}} \gtrsim 3$ ) and was followed by passive evolution of the stellar populations, whereas in the hierarchical assembly scenario the timescales for more massive galaxies are longer, resulting in somewhat younger mean ages. According to the latter interpretation, ellipticals are formed by mergers and/or accretion of smaller galaxies over timescales comparable to the Hubble time (see e.g. Bell et al. 2004; Faber et al. 2005).

Fundamental observational constraints on the star for-

mation history and the formation pattern are provided by the broad-band colours, line strength indexes and stellar chemical abundances. When referred to massive ellipticals, these data suggest that the bulk of stars might have been formed in a remote past. However, some secondary activity of star formation in the recent past is also evident: nearby ellipticals show a large variety of morphological and kinematic peculiarities (e.g. Longhetti et al. 2000) and a substantial spread of stellar ages, particularly for the field population (Thomas et al. 2005). Strong evolution in the population of early-type galaxies has been reported by Kauffmann et al. (1996) and Kauffmann & Charlot (1998) which has been considered to support the hierarchical galaxy formation models.

The current results about the number counts and redshift distributions of the evolved galaxies at high redshift are still rather inconclusive, and theoretical models about their formation and evolution are correspondingly uncertain (see Somerville et al. 2004 for a brief review).

Near-infrared surveys are best suited for the study of faint high-redshift galaxy populations, for various reasons: the observed fluxes are minimally influenced by K-corrections and only weakly affected by dust extinction, and at the same time good indicators of the stellar mass content of galaxies (Dickinson et al. 2003). Mid-infrared observations, on their side, are strongly informative about phases of active star formation in galaxies (Franceschini et al. 2001; Rowan-Robinson 2001; Xu et al. 2003 and many others). After the ISO exploratory observations, the Spitzer Space Observatory mission has started to map systematically the high-redshift universe at such long wavelengths.

The main aim of the Spitzer Wide-area InfraRed Extragalactic survey (SWIRE) is the study of the evolution of both actively star-forming and passively-evolving galaxies, by exploiting a huge sample of some 2 million galaxies that are detected within the  $\sim 50$  deg<sup>2</sup> of the survey.

Good quality optical data are essential for the identification and characterization of Spitzer sources. However, typical images obtainable from the ground are not adequate for accurate morphological analysis and source classification. In this paper we exploit very deep multiband public images taken with the Advanced Camera for Surveys (hereafter ACS; Ford et al. 1998) in a small portion of the SWIRE N1 field, in order to study the morphological properties of the infrared (IR) emitting galaxies. In what follows and unless specified otherwise, IR refers to 3.6 and 4.5  $\mu$ m.

Section 2 of the paper describes the optical (HST/ACS) and IR (Spitzer) data used in our analysis. Section 3.1 gives a brief description of the tools used for the morphological analysis and classification as well as a comparison of their results. Section 4 describes a comparison of our modelistic galaxy number counts with our observational data. Finally, sections 4.3 and 5 summarise our results and conclusions.

## 2 THE DATA

SWIRE N1 was the first field to be observed by Spitzer for the SWIRE Legacy program. The IR data used here were obtained in February 2004 and the SWIRE catalogues we use throughout this work were processed by the SWIRE team. Source extraction was performed using *SEtractor*

(Bertin & Arnouts 1996) with local background mesh subtraction. Kron and 2.9" aperture fluxes were used here, for extended and point-like sources, respectively. The Kron fluxes were extracted within a minimum radius of 2" using a Kron factor of 2.5. These fluxes were the *default* fluxes in the first SWIRE data release. The 3.6 and 4.5  $\mu$ m counts are roughly 90% complete at around 10  $\mu$ Jy. The astrometric accuracy is better than 1". More details about the entire data set can be found in Lonsdale et al. 2004, Surace et al. (in preparation) and Shupe et al. (in preparation), as well as the data release document (Surace et al. 2004).

The optical data were obtained with the ACS on the Hubble Space Telescope. The field is centred on UGC 10214 (also known as VV 29 and Arp 188, the *Tadpole* galaxy), a bright spiral at  $z = 0.032$  with a huge tidal tail. The optical catalogue contains some 5700 objects with 10  $\sigma$  detection limits for point sources of 27.8, 27.6 and 27.2 AB magnitudes in the  $g_{F475W}$ ,  $V_{F606W}$  and  $I_{F814W}$  bands respectively. For details on the data reduction and catalogue production see Benitez et al. 2004. This field lies close to the centre of the SWIRE N1 field, providing an unprecedented opportunity of combining very deep optical data with high quality IR data in wavelength ranges so far poorly explored.

Within the  $\sim 14$  sq. arcmin ACS field, we use an area of  $\sim 10$  sq. arcmin well outside the region occupied by the UGC 10214 galaxy. Any remaining background contamination likely to affect the IRAC fluxes is accounted for thanks to the way the SWIRE catalogues are created: they use a locally generated background estimate and any underlying faint extended emission is considered as background and subtracted.

The matching between the SWIRE and ACS sources was done using the *TMATCH* task of *IRAF*, with an 1" match radius. The sources were then visualised one by one and a flag was assigned to each one of them, stating their status with respect to close counterparts. Out of the 177 matched objects, 175 and 130 are detected in 3.6 and 4.5  $\mu$ m, respectively (with two having only 4.5  $\mu$ m detections) and 18 (i.e.  $\sim 10\%$ ) have at least two extracted ACS counterparts within an 1" radius. For six of them, however, we can clearly identify the object that mostly contributes to the IRAC fluxes, as the difference in I-band magnitude between the counterparts is larger than 2.5. For a detailed discussion of the optical/IR bandmerged catalogues and the spectral energy distribution (SED) of the matched objects we defer to Pérez-Fournon et al. (in preparation) and Hernán-Caballero et al. (in preparation).

The I-band counts for the entire ACS field and for the sources with a SWIRE counterpart are shown in Fig. 1 in solid and in dashed lines, respectively. Down to a magnitude of  $I \sim 22.5$  almost all ACS sources have an IR counterpart, while the number starts dropping below  $I \sim 23.5$ , reflecting the shallowness of the SWIRE data. The completeness of the 3.6  $\mu$ m counts drops quickly below 10  $\mu$ Jy, value corresponding to an AB limiting magnitude of 21.4 or  $I \sim 23.5$  for a typical I-3.6 $\mu$ m colour of 2 (see Fig. 2 for the colour distribution of the 177 matched sources).

Note that the probability of chance associations within 1" of radius is of less than 2% up to an I-band magnitude of 24.0 and up to 5% at an I-band magnitude of 25. Taking into account the I-band magnitude distribution of the

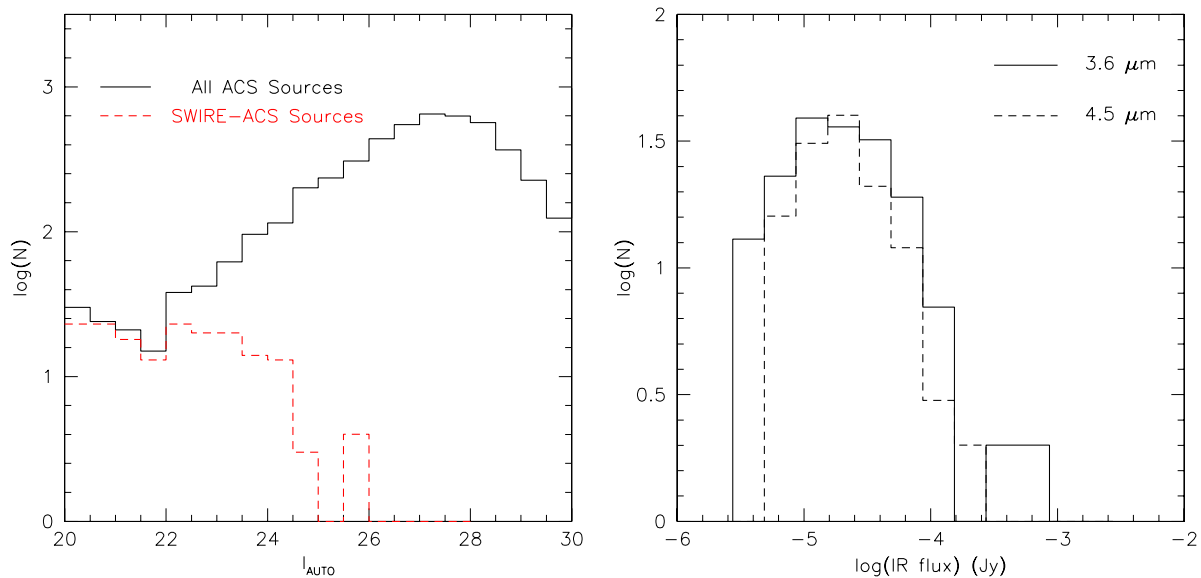


**Figure 1.** Left panel: I-band number counts for all ACS sources (solid line) and for the SWIRE-ACS identifications (dashed line) in the  $\sim 10$  sq. arcmin field covered by the ACS observations, after the area around UGC 10214 has been removed. Right panel:  $3.6 \mu\text{m}$  (solid line) and  $4.5 \mu\text{m}$  (dashed line) distribution of the SWIRE-ACS sources.

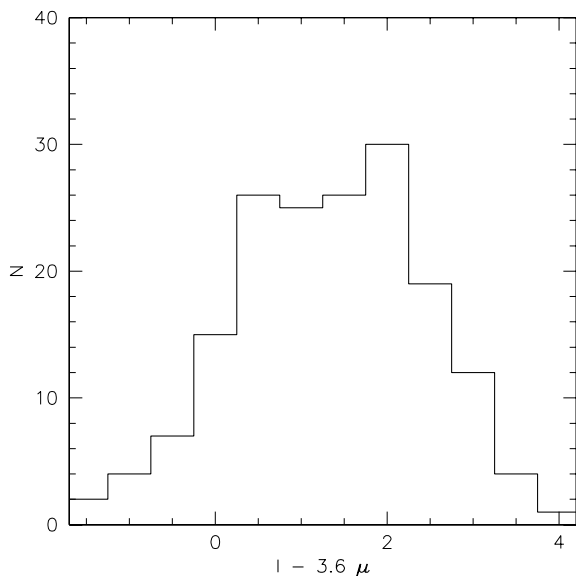


**Figure 2.**  $(I-3.6\mu\text{m})_{AB}$  colour histogram for the matched SWIRE-ACS sources.

SWIRE sources (Fig. 1), one expects less than 5 out of the 177 sources to be wrongly matched.

### 3 MORPHOLOGICAL CLASSIFICATION

#### 3.1 Tools for the morphological analysis

A number of parametric and non-parametric methods are suggested in the literature for quantitative assessment of the morphological properties of intermediate and high redshift galaxies. Among the parametric approaches, an often

used representation of the galaxy morphological types is the Sérsic index,  $n$ , which appears in the surface brightness profile law  $I_r = I_b(0)e^{-b_n(r/r_m)^{1/n}}$ , where  $I_b(0)$  is the bulge central intensity,  $r_m$  is the bulge semi-major effective radius and  $n$  the Sérsic shape parameter (Sérsic 1968). The quantity  $b_n$  is a function of  $n$ , and is chosen so that  $r_m$  encloses half of the total luminosity. The Sérsic profile includes the classical de Vaucouleurs profile when  $n$  is equal to 4.

Alternatively, non-parametric approaches have been proposed, with the most common one using the combination of the light Concentration ( $C$ ), Asymmetry ( $A$ ) and clumpiness ( $S$ ), or CAS, parameters. Concentration (Abraham et al. 1996) roughly correlates with the Sérsic index, while asymmetry (Conselice et al. 2000) compares the image of a source with its rotated (usually by  $180^\circ$ ) counterpart, enabling the distinction between normal and irregular galaxies or merging systems. The clumpiness, (Conselice 2003), measures the uniformity of the light distribution in a galaxy. Abraham et al. (1996) and later on (Conselice et al. 2000) showed that bulge-dominated, disk-dominated and merging systems occupy different but often overlapping regions in the Asymmetry - Concentration space. Conselice (2003) finally demonstrated that all galaxy types can be roughly identified by their position in the CAS three-dimensional space.

Our morphological analysis has been performed in three independent steps: i) visual inspection, in order to attribute each object to a given morphological class based on features like the presence of spiral arms and/or bars, signs of interaction, multiple nuclei etc; ii) a non-parametric analysis of the galaxy light distribution using the CAS parameters (see Conselice et al. 2003 for a detailed description and Cassata et al. 2005 for their exact definition as used here); iii) a detailed analysis of the surface brightness profiles using

the packages GALFIT (Peng et al. 2000) and GASPHOT (Pignatelli et al. 2005).

### 3.2 Results of the morphological analysis

In the 10.56 sq. arcmin region of the ACS field uncontaminated by UGC 10214, there are 177 objects with a SWIRE counterpart. As a first step, a visual inspection of these sources was carried out on the I-band image by three of the authors, independently. The individual results were then compared and finally combined after the very few dubious cases were discussed (the excellent quality of the ACS data allows for very little doubt about the morphological characteristics of the objects at these relatively bright magnitudes). The visual analysis identifies four main groups of objects: *spheroids* (consisting of ellipticals and S0 galaxies), *spirals*, *irregular* galaxies and *pairs* and found four objects too faint to be classified; 21 were stars (stars were double-checked adopting the criterion of Benitez et al. 2004 for stellar classification, i.e. a SExtractor CLASS\_STAR  $\geq 0.94$ ); 37 spheroids; 69 spiral galaxies; 24 irregulars and 22 merger or interacting systems or sources with multiple components (all characterised as *pairs*). Fig. 3 shows examples of each of the categories along with their CAS parameters, discussed hereafter.

For nearly a quarter of the 156 galaxies (the 21 stars are from now on excluded), CAS parameters were not computed. Before computing CAS, pixels below  $2 \times \text{RMS}$  are filtered out (corresponding to  $25 \text{ mag/arcsec}^2$ ). For objects with no pixels above this level the  $A$  and  $S$  are not computed. The computation of  $C$  makes use of the SExtractor-derived growth curve of each object and no filter is applied on the image. For objects with complex structure (visually classified as pairs or irregular galaxies), their multiple components or uncommon shape render the CAS analysis difficult. For the rest of the sources, however, this approach gave results largely in agreement with the visual inspection. Spheroids tend to have lower  $A$  and higher  $C$  than spirals, irregulars or pairs and tend to concentrate around  $S \sim 0.1$ . In fact, 36 of the 37 visually classified spheroids lie in or at the very borders of the region shown in Fig. 4, defined by:

$$A < 0.2 \ \& \ C > 2.7 \quad (1)$$

$$C > 2.7 \ \& \ 0.0 \leq S < 0.3 \quad (2)$$

$$0.0 \leq S < 0.3 \ \& \ 3A - S < 0.3 \quad (3)$$

An additional set of 10 objects fall within this same region. Those objects are spirals but at least seven of them have prominent bulge components, as seen on the cutouts illustrated in Fig. 5. Note that for some of them it is difficult to see the spiral arms or disk components on the cutouts due to the chosen contrast but they are clear enough on the actual image for the objects to be classified as spirals. We therefore deduce that more than 93% of the objects in the designated area of the CAS parameter space are ellipticals or bulge-dominated spirals (lower limit if one considers the 36 ellipticals and the seven clearly bulge-dominated spirals among the 46 objects lying in this area).

This analysis sets the lower and upper limits of the number of spheroids in 37 (visually classified) and 46 (included in the region delineated by Eqs. 1-3), respectively, within

the  $\sim 10$  sq. arcmin of effective area of the UGC 10214 ACS field.

The results of the parametric methods are more difficult to interpret. For low asymmetry objects the results of GALFIT and GASPHOT are in reasonable agreement with each other (Fig. 6) but discrepancies arise for the objects with  $A > 0.25$ . This is somewhat expected as the less symmetric galaxies can not be easily reproduced by parametric models that are intrinsically symmetric (see Cassata et al. 2005 and Pignatelli et al. 2005 for further details on the comparison between GASPHOT and GALFIT on real and simulated galaxies, respectively). Some 80% of the objects have  $\Delta n / \langle n \rangle$  less than 0.5, region indicated by the dashed lines on Fig. 6. Note that for some of the objects the two codes failed to converge and therefore do not appear on this plot (31 for GALFIT and 25 for GASPHOT, with 20 objects in common between the two failing groups). Parametric and non parametric approaches also agree up to a point, with the Sérsic index,  $n$ , correlating with  $C$  in the majority of the cases (Fig. 7). Some 15 sources, however, present large deviations. For these objects the errors on the estimated values of  $n$  are very large due to their nature: they are all pairs, sources with multiple components or (just one case) objects with very small isophotal area.

The distribution of Sérsic index,  $n$ , given by GALFIT is roughly bimodal, culminating at a value around 1 for late-type and around 2 for early-type galaxies. However, one third of the galaxies visually classified as early types have an  $n$  lower than 2, and about the same fraction of late-type galaxies have  $n$  greater than 2, implying that using a classification criterion based on the Sérsic index alone (see e.g. Ravindranath et al. 2004) would result in a certain amount of mis-classifications. Among the early type galaxies with a low value of the Sérsic index, a large fraction are S0 galaxies while a certain number have a too small isophotal area to get reliable fits of the surface brightness distribution. Finally, the largest part of late-type galaxies having large Sérsic indexes is mostly composed by bulge dominated systems or again objects occupying too small isophotal areas. Note that there was no lower limit imposed on the isophotal area in order to perform the fits, however all objects for which the fit failed to converge consisted of less than 50 pixels.

The entire morphological analysis may be subject to an, unaccounted for, morphological K-correction. Morphological classification performed at a given band suffers from this effect as galaxies of higher redshifts are actually observed at bluer restframe wavelengths (Windhorst et al. 2002; Papovich et al. 2003; Cassata et al. 2005). Windhorst et al. (2002) found that the morphology of galaxies changes when moving from the optical to the UV passbands. However, our analysis should not be much affected by this effect as we do not expect a large number of high redshift galaxies, due both to the relatively bright fluxes and to the very small size of the field. This, in fact, somewhat insures that we study galaxies with restframe between B- and I- bands. In particular, the number of high-redshift spheroids, population we are mostly interested in, must be particularly low. Rowan-Robinson et al. (2005), based on photometric redshift estimations and model predictions, showed that no more than 25% of the  $3.6 \mu\text{m}$  galaxy sample down to a limit of  $10 \mu\text{Jy}$  have redshifts larger than  $\sim 1$ , the largest fraction of which are late-type objects. CAS analysis may also suffer

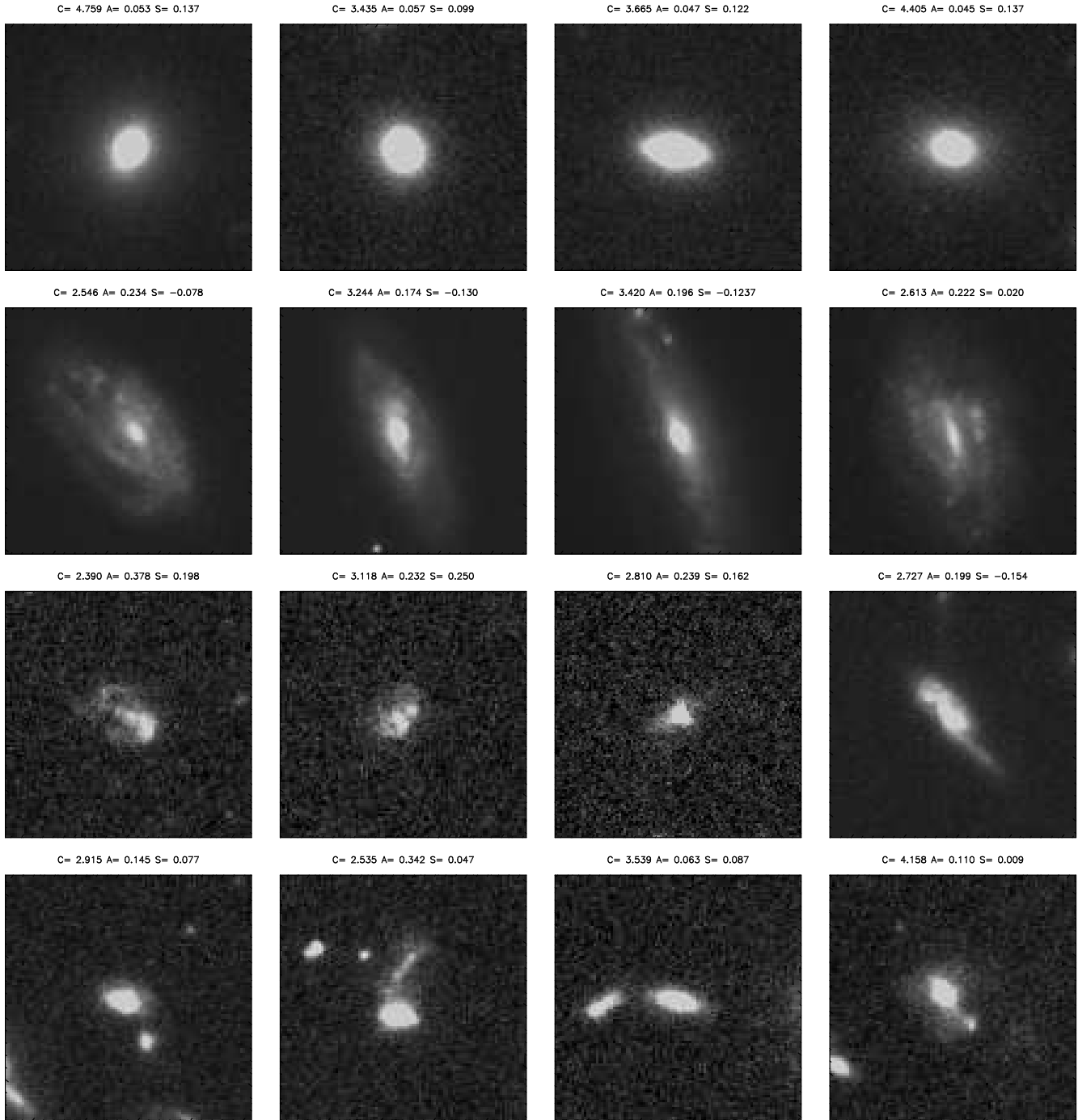


**Figure 3.** Examples of objects visually classified as ellipticals, spirals, irregulars and pairs (from upper to lower row) and their CAS parameters. The size of the cutouts is of  $5 \times 5$  arcsec.

from the effects of the morphological K-correction (see i.e. Conselice et al. 2000; Lotz et al. 2004), as in general, moving toward shorter wavelengths results in larger values of  $A$  and  $S$  and smaller  $C$ . However, since we ignore the real redshifts of our objects and decided not to rely upon the photometric redshifts provided by Benitez et al. (2004) – calculated based on three optical passbands only – in order to avoid introducing further uncertainties, we chose not to apply any kind of correction.

Finally, the effects of the aperture on the estimation

of the CAS parameters have not been considered here. The parameter most sensitive to the size of the aperture is  $A$  (Conselice et al. 2000) and is more likely to be affected in the case of faint, high-redshift objects. However, since much of our analysis is based on the  $C$  parameter and since the vast majority of our objects have very bright ACS counterparts (see Fig. 1, left panel), we are confident that aperture effects do not bias our work. The fact that visual inspection and CAS analysis are in such a good agreement when selecting early-type objects is also in support of our argument.

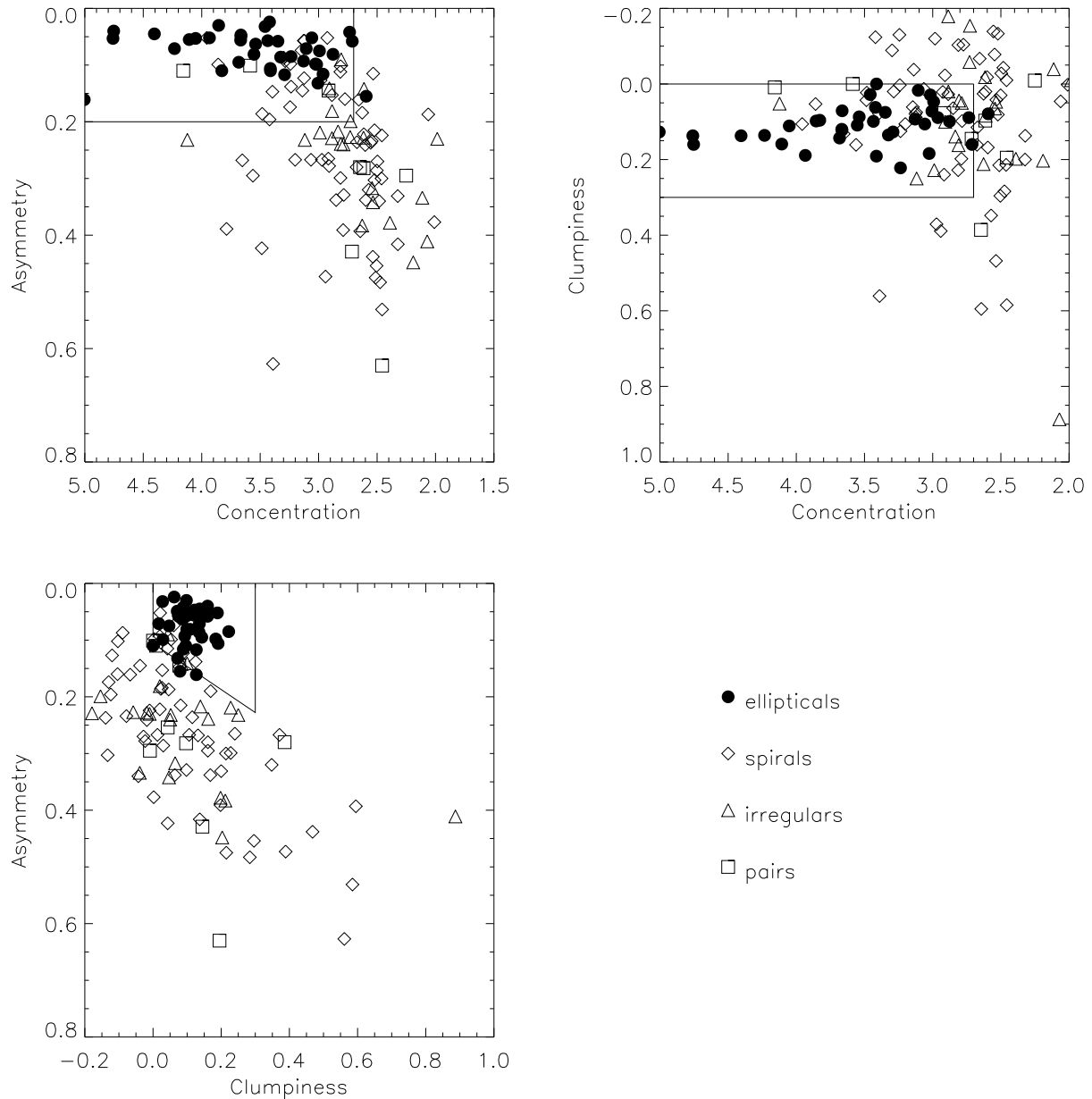


**Figure 4.** Asymmetry, Concentration and Clumpiness for the SWIRE-ACS galaxies and comparison with the classification obtained by visual inspection.

## 4 GALAXY NUMBER COUNTS

### 4.1 Observed number counts

The IRAC1 and IRAC2 channel (3.6 and 4.5  $\mu\text{m}$ ) observed cumulative galaxy counts are reported in the left column of Fig. 8. The various morphological classes are these derived from the visual inspection. We now confine our analysis to fluxes brighter than 10  $\mu\text{Jy}$  in the two bands, and assume that the sample is 90% complete here. This flux-limited sample consists of a total of 109 galaxies among which 28 are spheroids.

It is interesting to note here that the IRAC channels 1 & 2 are optimally suited for the identification and analysis

of spheroidal galaxy populations. We have performed an automated analysis of the I-band images over entire ACS field using the CAS parameter set and found that only  $\sim 7\%$  of the galaxies to the survey limit  $I=27.2$  lie in the area defined by Eqs. 1 – 3, and are therefore classifiable as spheroids. The same analysis performed on the counterparts of the SWIRE IRAC population shows a much larger incidence ( $\sim 20\%$ ) of early-type galaxies. This is the result of the IR selection, favouring the detection of galaxies with old stellar populations. Deeper SWIRE observations might reveal later type IR counterparts of the ACS sources, however this is not evident from the actual distribution of morphologies of the IRAC sources with the I-band magnitude: the percentage

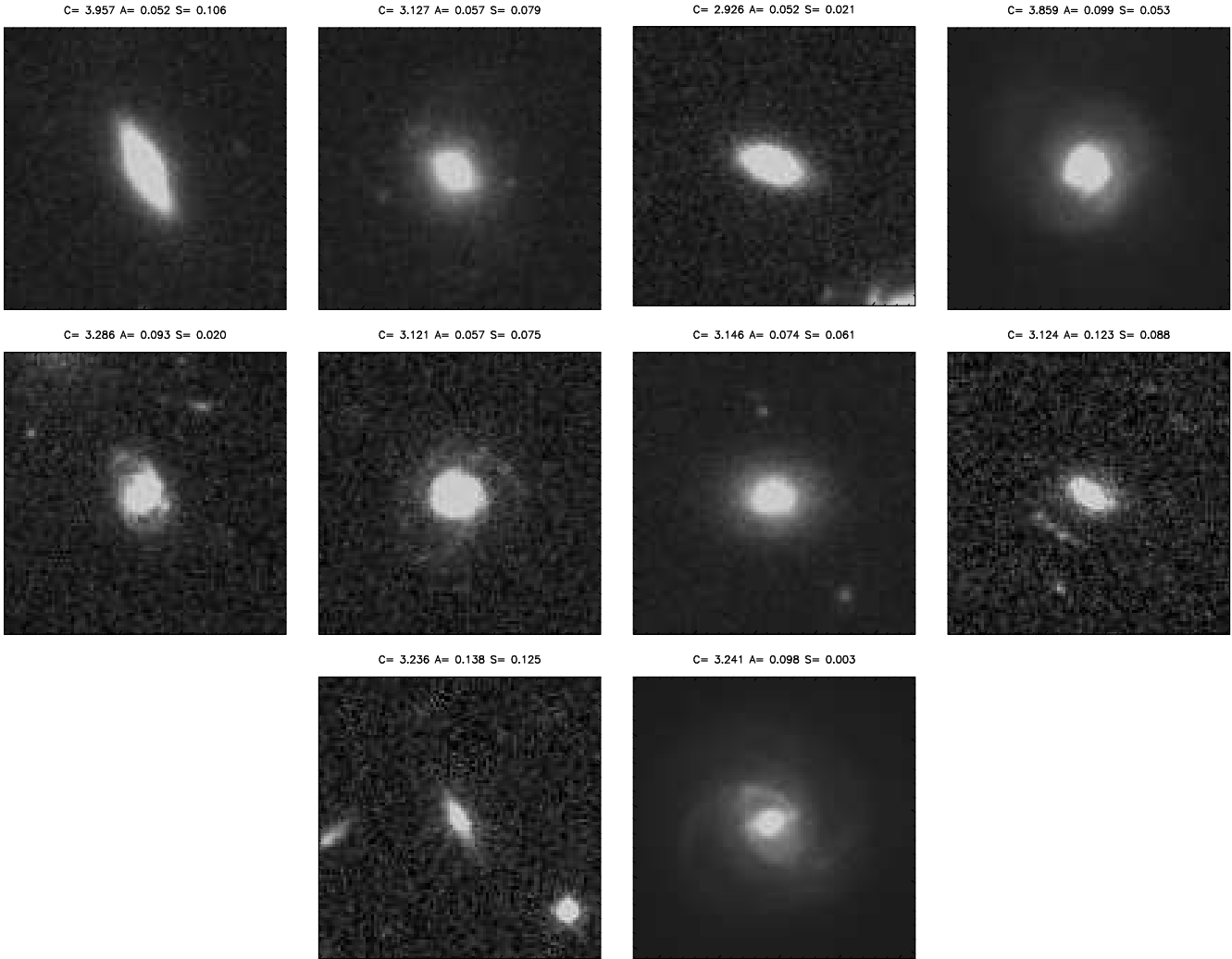


**Figure 5.** The ten galaxies visually classified as spirals that lie in the *CAS* spheroid region.

of early-type objects in bins of magnitude in the interval  $[19.0, 25.0]$  takes values between 15% to 45% but without demonstrating any specific trend.

#### 4.2 Model number counts

We now compare the statistical observables derived from our Spitzer IRAC dataset with simple evolutionary models. While the details on the models are more extensively described in Rodighiero et al. (2005, in prep.), we provide here a summary of our general approach. We adopt in the following  $H_0=70$ ,  $\Omega_M=0.3$ ,  $\Omega_\Lambda = 0.7$ .

In our approach four main galaxy classes are considered: spheroids, quiescent spirals, an evolving population of irregular/merger systems (hereafter starburst population), and minor contributions from AGN.

The SED templates describing the spectral shapes at different galactic ages, needed to calculate the K-corrections, have been computed using the stellar population synthesis code GRASIL (Silva et al. 1998). We adopt a Salpeter IMF with a lower limit  $M_l = 0.15M_\odot$  and a Schmidt-type law for the star formation (SF) rate:  $\Psi(t) = \nu M_g(t)$ , where  $\nu$  is the

efficiency and  $M_g(t)$  is the residual mass of gas. A further relevant parameter is the timescale  $t_{infall}$  for the infall of primordial gas. The evolution patterns for the models considered here are obtained with the following choices of the parameters. For early-types:  $t_{infall} = 1 \text{ Gyr}$ ,  $\nu = 1.3 \text{ Gyr}^{-1}$ ; for late-types:  $t_{infall} = 4 \text{ Gyr}$ ,  $\nu = 0.6 \text{ Gyr}^{-1}$ . The corresponding SF law for ellipticals have a maximum at galactic ages of 1.4 Gyr, and is truncated at 3 Gyr to mimic the onset of a galactic wind. For late-type galaxies, the peak of the SF occurs at 3 Gyr. The parameters assumed to reproduce the spectra of spirals and irregular galaxies are that of a typical Sb spiral. This may not be very representative of an evolving population during a starburst phase, however, given the spectral region considered in this work, our assumption is still a good approximation. We have then generated two grids of model SEDs for both early- and late-types, spanning a range of ages from 0.1 to 15 Gyr. For what concerns the spheroids, we made the assumption that these stellar systems are gas and dust free, so that extinction is negligible. Extinction is instead considered for late-type galaxies, with an evolution of the dust to gas ratio typical of an Sb galaxy (we assume the parameters proposed by Silva et al. (1998)).

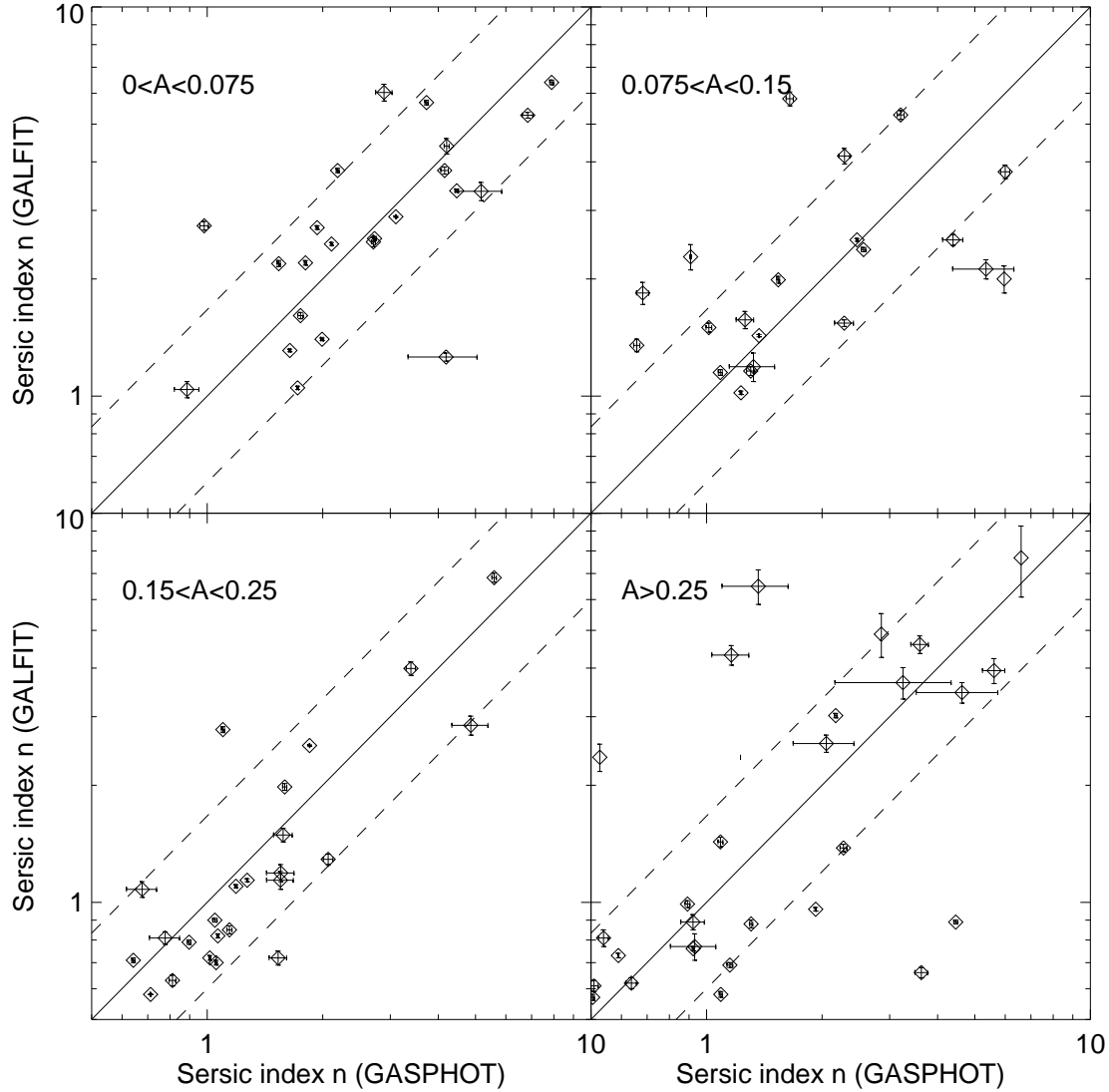


**Figure 6.** Sérsic index,  $n$ , computed by GALFIT versus  $n$  computed by GASPHOT for the SWIRE-ACS galaxies, in bins of Asymmetry. The two tools provide comparable results for low asymmetry objects. The dashed lines mark the region where  $\Delta n/\bar{n} \leq 0.5$ , occupied by  $\sim 80\%$  of the objects. Objects with  $n < 0.5$  - 22 in total - or objects for which one of the methods did not converge are not shown.

Heated dust possibly contributes to the emission from the late-type galaxies at rest-frame wavelengths longer than 2-3  $\mu\text{m}$ , which could effect the derived model flux densities in the IRAC bands. This will be considered in a future work.

For the local luminosity function we have made use of that estimated by Kochanek et al. (2001) for both early-type and late-type galaxy classes and derived from a K-band selected sample taken from the Two Micron All Sky Survey (2MASS), including 4192 low-redshift ( $z \sim 0.02$ ) galaxies.

Our schematic model for both the spheroidal and the spiral population assumes that the galaxy comoving number density keeps constant once the population is formed at a

given redshift, while the galaxy luminosities evolve following their evolutionary stellar content.

On the other hand, the analysis of deep galaxy surveys in the K-band (Cassata et al. 2005; Franceschini et al. 2005 in prep.) indicates the presence of a numerous population of irregular/merging systems at high-redshifts, likely requiring luminosity as well as density evolution going back in cosmic time. We then add a population of starbursts whose density  $\rho(z)$  evolves with the following rule:

$$\rho(z) \propto \rho(z_0) \times (1+z) \quad (4)$$

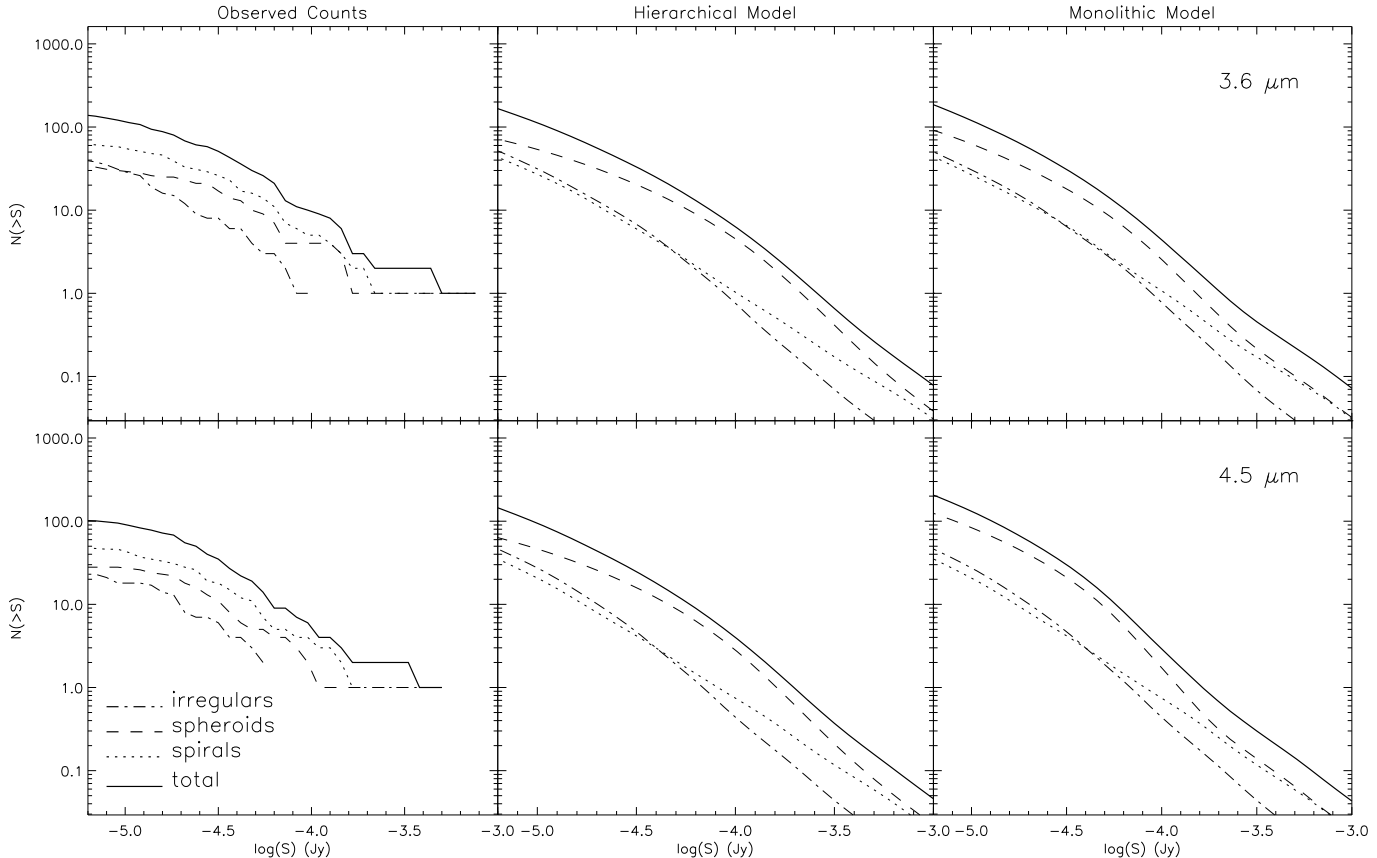


**Figure 8.** Left column: observed cumulative 3.6 (upper panel) and 4.5  $\mu\text{m}$  (lower panel) counts for the various types of objects (as classified by visual inspection) and their total number (solid line). Middle and right columns: cumulative model counts for the *hierarchical* (middle) and *monolithic* (right) models. The counts are reported here for the various different morphological classes as indicated in the line caption. Note that *monolithic* and *hierarchical* scenarios only differ in the spheroids’ (and therefore also total) counts.

for  $z < 1$ , and constant above, and whose luminosities  $L(z)$  increases as

$$L(z) \propto L(z_0) \times (1+z)^{1.3} \quad (5)$$

for  $z < 2$ , and constant above.

Before detailing the comparison of our model predictions with the observed statistics derived from our sample, we need to consider how a morphological selection correlates with a classification based on the intrinsic SED of galaxies. A convenient way to directly check this point is to look at the colours of the SEDs templates assumed by the model, in order to verify if they are representative of the morphologically selected spheroids and spiral populations.

As an example, in Fig. 9 we report the I-4.5  $\mu\text{m}$  versus the g- 3.6  $\mu\text{m}$  observed colour-colour plot, compared with the evolutionary tracks derived using model templates. The blue dots mark the visually classified late-type sources; red open circles are spheroids; green triangles are galaxy pairs. The curves show the evolutionary tracks corresponding to elliptical and spiral SEDs at different ages (thick red solid - dotted - dashed lines: ellipticals of 1, 2 and 10 Gyr, respectively; blue solid - dotted - dashed - long dashed: 3, 5, 10 and 15 Gyr, respectively), spanning the redshift range between 0 and 1.8. Fig. 9 suggests that morphologically selected elliptical galaxies preferentially populate the reddest region of

the observed colour distribution. However, the colour degeneracy between age and extinction prevents us from having an unambiguous photometric selection for spheroids. This can also be seen on this figure, where spheroids and late-type galaxies occupy contiguous and partially overlapping regions of the colour-colour space. The above mentioned degeneracy between age and extinction have thus produced star-forming sources with observed red colours (generally attributed to old stellar systems). Similarly, those spheroids that have undergone recent episodes of star formation have bluer colours and then fall within the region preferentially populated by late-types.

This analysis suggests that a pure morphological selection is not obviously comparable with a colour criterion, and that a given amount of contamination affects such kind of comparison. However, assuming that the template SEDs discussed above are reasonably representative of the morphological classes, we have investigated the statistical properties of the SWIRE sample and compared them with the model predictions. Any conclusion based on this analysis has to be taken with caution, in particular for the specific properties of the different spheroidal and spiral/irregular classes.

We now explore two schemes for the formation of spheroidal galaxies. The first one corresponds to the classic – *monolithic* – scenario assuming a single impulsive episode

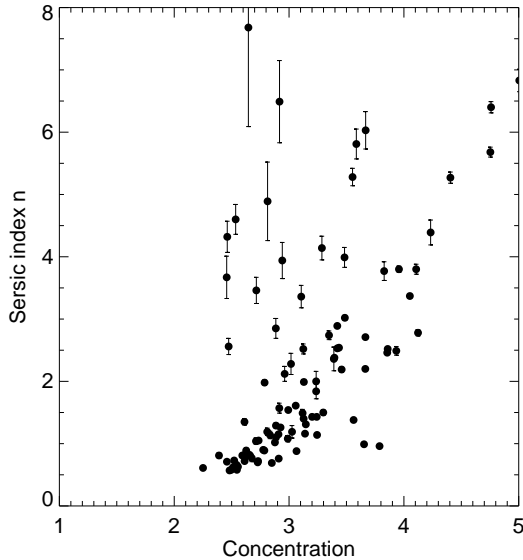


**Figure 7.** Sérsic index,  $n$ , computed by GALFIT versus Concentration,  $C$ .  $n$  scales with  $C$  in the majority of cases. The objects with the largest scatter are also those with the largest error bars and, in the majority of cases, have been visually classified as pairs (including systems with various components).

for the formation/assembly of the field ellipticals, occurring at a high redshift ( $z_{\text{form}} > 2.5$ , e.g. Daddi et al. 2000 and Cimatti et al. 2002). In our current implementation, we assume a redshift of formation  $z_{\text{form}} = 3.0$ . In this single burst model the birth of the stellar populations is coeval to the formation of the spheroids.

The second model for spheroidal galaxies – the *hierarchical* model – describes a situation in which massive ellipticals form at lower redshifts through the merging of smaller units down to recent epochs. In such a case the formation of early-type galaxies is spread in cosmic time. Very schematically, we achieve this by splitting the local spheroidal galaxies into several sub-populations, each one forming at different redshifts (in coincidence with the birth of a new populations of stars building up the younger spheroids). All sub-populations have the same mass function but different normalizations, whose total at  $z = 0$  has to reproduce the local luminosity function. This model is being tested against deep galaxy surveys in the K-band, showing a general tight agreement between predictions for the different morphological classes and observations (K20 Cimatti et al. 2002, HDFs Franceschini et al. 1998 and Rodighiero et al. 2001; GDDS Abraham et al. 2004). In our current implementation, the bulk ( $\sim 60\%$ ) of the early-type mass function is dynamically assembled in the redshift interval  $1.1 < z < 1.6$ , with additional fractions being assembled at higher and lower  $z$ . At this stage, and for simplicity, we do not consider extinction effects during the star formation phase of the spheroids. We defer to Franceschini et al. (2005) and Rodighiero et al. (2005) for a more detailed discussion and additional applications of this modeling.

Fig. 8 shows the predicted cumulative number counts at for the hierarchical (middle panel) and monolithic (right panel) scenario, respectively. The difference is essentially in

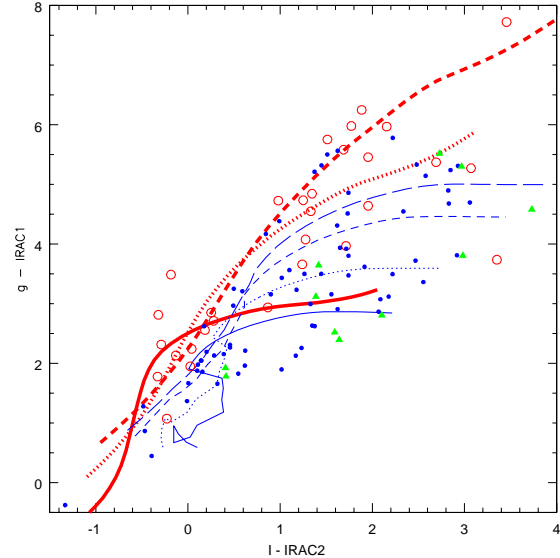


**Figure 9.** Colour-colour diagram ( $g$ -IRAC1) vs ( $I$ -IRAC2) showing the location of the spheroids, spirals and pairs (in open circles, dots and filled triangles, respectively) and the model evolutionary tracks of ellipticals and spirals of various ages (in thick red and thin blue lines, respectively; for details about the line coding, see text).

the spheroidal population. The main value of these models is to provide, particularly for the spheroidal and normal spiral components, the simplest possible extrapolations of the local luminosity functions back in cosmic time. The addition of a strongly evolving population of irregular/mergers is instead motivated by the need to reproduce, at least at the zeroth order, the observed statistics from deep K-band counts (Franceschini et al. 2005). In any case, these simple models predict that spheroidal galaxies would make important contributions to the Spitzer/IRAC counts at fluxes above 10  $\mu\text{Jy}$ .

### 4.3 Discussion

We report in Figs. 10 and 11 detailed comparisons, with model expectations, of the SWIRE observed integral counts at 3.6 and 4.5  $\mu\text{m}$  for the various morphological classes in the *Tadpole* ACS image. Only a general distinction between spheroidal and non-spheroidal systems is made here, the latter including both spirals and irregulars/mergers. The observed counts are shown down to 10  $\mu\text{Jy}$ , roughly the 90% completeness limits of SWIRE IRAC1 band. The solid and dashed lines correspond to the hierarchical and monolithic scenario, respectively, while the dotted lines show the observed number counts. More precisely, the two dotted lines appearing in these figures for each morphological class correspond to the lower and upper boundaries on the source real density which have been discussed in Sect. 3.2. The upper and lower limits in this case of spheroids correspond to the CAS analysis and visual inspection, respectively, whereas in the case of the remaining classes (marked in the plot as “other”) the upper limit is due to visual inspection and the lower to the CAS parameters. The observed IRAC1

counts given by Fazio et al. (2004) are shown for comparison (marked as diamonds in Figs. 10 and 11). Note that, given the modest statistics of our source sample, the detailed shapes of the counts (showing bumps and humps at the bright end of the counts) are not to be considered as significant.

Despite the very small size of our sample, the total counts are in good agreement with those observed by Fazio et al. (2004) over a much larger area (several square degrees), especially the  $3.6\ \mu\text{m}$  counts. In the case of the  $4.5\ \mu\text{m}$  counts, the statistics start being really poor as we are dealing with only 104 objects detected in this band down to the adopted flux limit. The observed spheroidal counts are in very good agreement with those predicted by the hierarchical scenario while the monolithic model suggests steeper counts. However, while the models predict counts essentially dominated by ellipticals (see middle and right panels of Fig. 8), we observe an excess of late-type galaxies and merger-irregulars to dominate the counts. Comparison between this same model and K-band observations did not show any discrepancy.

The observed spheroids counts are inconsistent with the monolithic predictions that implies too steep number counts and would not only exceed the observed counts at the faint fluxes but also underpredict the bright end  $3.6\ \mu\text{m}$  counts. A coeval origin for spheroids at high redshift (i.e. formation of their stars in an instantaneous burst at  $z > 3$ ), therefore, seems to produce excess counts compared to observations. Changing the stellar IMF during the star-formation phase from a Salpeter to e.g. a Scalo (1986) distribution would probably somehow ease the inconsistency (Cimatti et al. 2002), but at the cost of not explaining by large factors the extragalactic background radiation intensities (Madau & Pozzetti 2000, Franceschini et al. 2001) and the observed metallicities of intracluster plasmas (Muskotzky & Loewenstein 1997).

On the other hand, the observed numbers of spiral and irregular galaxies are larger than that predicted by our simple evolutionary scheme. This simple model, consistently fitting the K-band galaxy statistics, falls short of the observed counts at both  $3.6$  and  $4.5\ \mu\text{m}$ . The rising of the contribution of the late-type population to the  $3.6$  and  $4.5\ \mu\text{m}$  emission, with respect to its contribution at  $2.2\ \mu\text{m}$ , might suggest a much stronger evolution (in both density and luminosity) for star-forming galaxies at longer wavelengths. Our results might indicate that the  $3.6\ \mu\text{m}$  band selects more active galaxies than the K-band ( $2.2\ \mu\text{m}$ ). If in the model the starburst and spiral populations are then assumed to contribute more significantly to the source counts, the discrepancy with observations should be reduced. Moreover, a more suited set of SED templates describing the star-forming population should be included (accounting for PAH emission and a more accurate description of dust and extinction, given that in our approach we roughly assume similar spectra for spirals and evolving starburst). However, larger sample and statistics are needed to check this assumption.

Very qualitatively, it might be tempting to interpret the observed excess population of irregulars and mergers and their inferred strong cosmological evolution as the progenitors of spheroidal galaxies, the rapid relaxation and gas exhaustion following the merger bringing to a sudden appearance of a spheroid. Obviously, any more quantitative

conclusion will require much further information on source identifications and redshifts.

Because of the inconsistency between observed and model late-type galaxies, we further compared our results with an improved version of the model presented by Xu et al. (2003). In its original version this model over-predicted the  $24\ \mu\text{m}$  counts at flux levels of  $\sim 1\ \text{mJy}$  (for a detailed discussion see Papovich et al. 2004 and Shupe et al. in preparation). In order to correct for this effect but still fit the  $15\ \mu\text{m}$  *ISO* counts the evolution rate of starburst galaxies was lowered with respect to the old model and the strength of the PAH features in the wavelength range of  $5\ \mu\text{m} < \lambda < 12\ \mu\text{m}$  was raised by a factor of 2 in the SEDs of both starburst and normal galaxies. Thus, the predicted late-type counts are still below the observed limits but are higher by a factor of  $\sim 1.5$  than those predicted by our simple hierarchical scenario. They are shown in dashed-triple-dot line in Figs. 10 and 11. This reinforces our previous statement about the deficit of model late-type galaxies reflecting the lack of PAH emission from the models presented in Section 4.2.

## 5 CONCLUSIONS

This work presents results of a morphological analysis of a small subset of the Spitzer Wide-area InfraRed Extragalactic survey (SWIRE) galaxy population. Our sample is flux-limited at  $3.6$  and  $4.5\ \mu\text{m}$  and consists of 156 galaxies. Our analysis is based on public ACS data taken inside the SWIRE N1 field. We distinguish two very general classes of galaxies, bulge- and disk- dominated ones, the first class being referred at with the general term “spheroids” and the second one containing everything from spirals to irregulars and pairs. Even though the requirement for  $3.6$  and/or  $4.5\ \mu\text{m}$  detections favours the selection of early-type galaxies, the sample under study is dominated by a large fraction of disk galaxies and interacting systems ( $\sim 80\%$ ), already suggesting that elliptical galaxies assemble late.

The *monolithic* and *hierarchical* models checked against this data set considerably under-predict the number of late-type galaxies. The observed  $3.6$  and  $4.5\ \mu\text{m}$  early-type counts are in very good agreement with the estimations of the hierarchical scenario, showing however a deficit toward the fainter end of the counts, possibly reflecting some incompleteness that is already introduced at this flux level. The monolithic predictions imply steeper counts and fail in reproducing the observations. The disagreement is stronger at the faint end of the  $4.5\ \mu\text{m}$  early-type counts.

Additional comparison of the dataset with another model available in the literature (Xu et al. 2003) suggested that dealing in an appropriate way with some of the models deficiencies like the dust or PAH emission components should result in a better agreement. It should be mentioned that the model predictions may depend significantly on the assumed stellar IMF (see e.g. Cimatti et al. 2002), although the one we adopted here should be rather representative of the main phases of star formation. The model itself is rough and the predicted counts should not be taken at face value but rather be considered indicative of the expected tendencies.

This ACS data set is the deepest available, as of today,

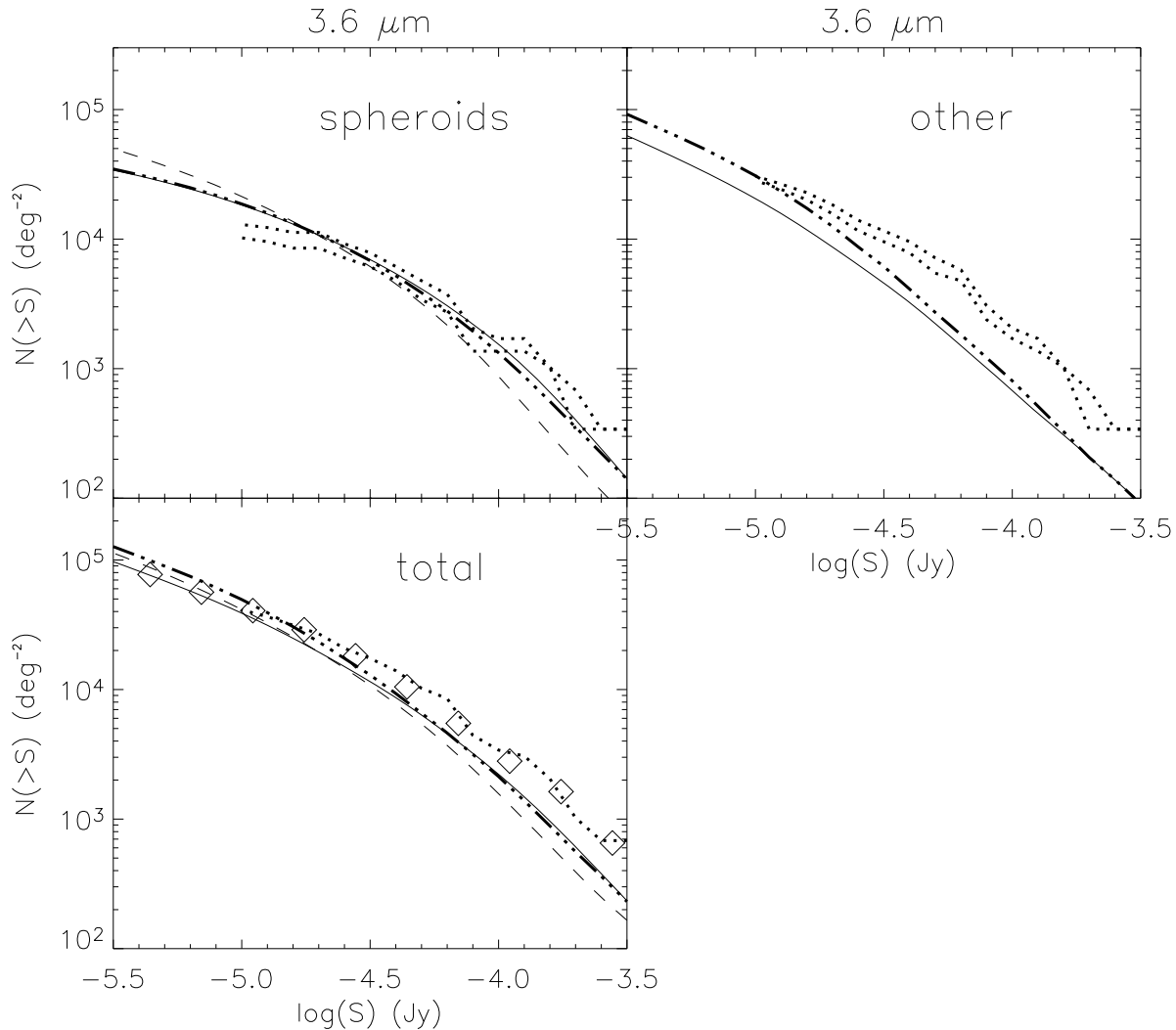


**Figure 10.** Comparison of the observed (dotted line) and model (solid and long-dashed lines for the hierarchical and monolithic scenario, respectively)  $3.6\ \mu\text{m}$  number counts. The upper and lower limits for the observed counts are given by the CAS parameter analysis and visual inspection, respectively, as discussed in the text. Note that, compared with Fig. 8, the spiral and irregular galaxies are here combined in the “other” class. The diamonds in the lower panel represent the IRAC1 counts given by Fazio et al. (2004). The dashed-triple-dot line shows the predictions of an improved version of the model presented in Xu et al. 2003 (see text for details).

in any of the SWIRE fields and therefore the results of the present analysis are of great importance for the understanding of the SWIRE galaxy population. Due to the small size of our sample, however, we cannot be very conclusive and can only outline some general tendencies. We would like to point out a number of potential sources of uncertainty in the interpretation of our results, namely: i) the way that large-scale structure may influence the results, given the particularly small size of the ACS field; ii) the possible existence of heavily obscured, by dust, ellipticals at the stage of their formation; iii) the assumption of *a priori* values instead of a  $\chi^2$  minimization on some of the model parameters; and finally iv) the uncertainties on the exact shape of the SEDs of the various galaxy types in these newly explored, IR wavelengths.

## ACKNOWLEDGMENTS

This work is based on observations made with the *Spitzer Space Telescope*, which is operated by the Jet Propulsion Laboratory, California Institute of Technology under NASA contract 1407. Support for this work, part of the Spitzer Space Telescope Legacy Science Program, was provided by NASA through an award issued by the Jet Propulsion Laboratory, California Institute of Technology under NASA contract 1407.

ACS was developed under NASA contract NAS 5-32865, and this research has been supported by NASA grant NAG5-7697. We are grateful for an equipment grant from Sun Microsystems, Inc. The Space Telescope Science Institute is operated by AURA Inc., under NASA contract NAS5-26555.

This work was supported in part by the Spanish Min-

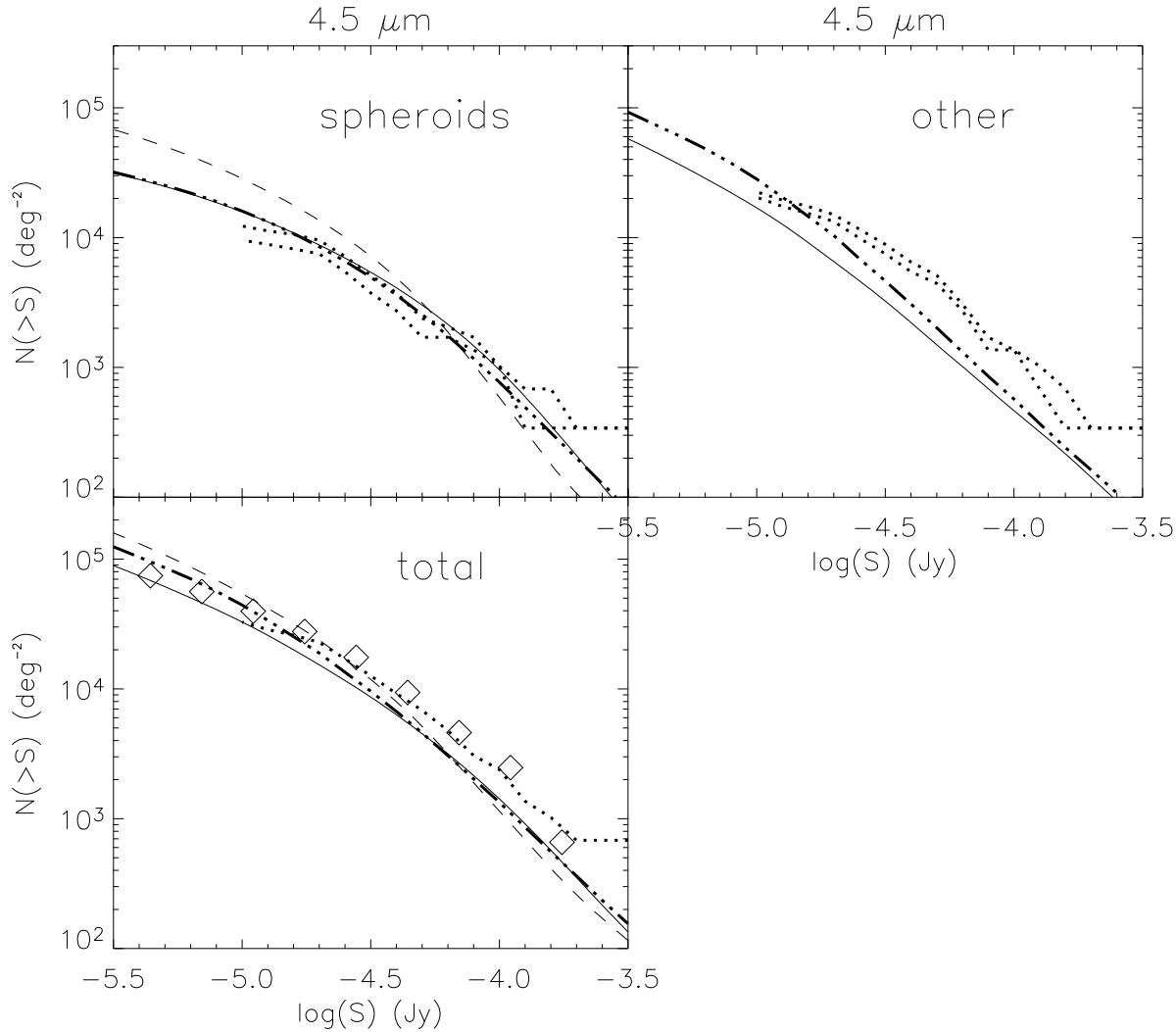


**Figure 11.** Same as Fig. 10 but for 4.5  $\mu\text{m}$ .

isterio de Ciencia y Tecnologia (Grants Nr. PB1998-0409-C02-01 and ESP2002-03716) and by the EC network "POE" (Grant Nr. HPRN-CT-2000-00138).

We would like to thank N. Benitez for making publicly available the reduced ACS image used in this work.

Finally we thank the anonymous referee for the precise and detailed report that greatly improved the presentation of our work.

## REFERENCES

- Abraham R.G., Tanvir N.R., Santiago B.X., Ellis R.S., Glazebrook K., van den Bergh S. 1996, MNRAS, 279, 47
- Abraham R.G. et al., 2004, AJ, 127, 2455
- Bell E. et al., 2004, ApJ, 608, 751
- Benitez N. et al., 2004, ApJ, 150, 1
- Bertin E., Arnouts S., 1996, A&AS, 117, 393
- Cassata P. et al., 2005, MNRAS, 357, 903
- Chiosi C., Carraro G., 2002, MNRAS, 335, 335
- Cimatti A. et al., 2002, A&A, 391, 1
- Cimatti A. et al., 2004, Nature, 430, 184
- Cole A., Lacey C.G., Baugh C.M., Frenk C.S., 2000, MNRAS, 319, 204
- Conselice C.J., Bershadsky M.A., Jangren A., 2000, ApJ, 529, 886
- Conselice C.J., 2003, ApJS, 147, 1
- Conselice C.J., Bershadsky M.A., Dickinson M., Papovich C., 2003, AJ, 126, 1183
- Daddi E., Cimatti A., Renzini A., 2000, A&A, 362, L45
- Dickinson M., Papovich, C., Ferguson, H.C., Budavari, T., 2003 ApJ, 587, 25
- Eggen O. J., Lynden-Bell D., Sandage A. R., 1962, ApJ, 136, 748
- Faber S.M. et al., 2005, ApJ submitted, astro-ph/0506044
- Fazio G.G. et al., ApJS, 154, 39
- Ford H.C. et al., 1998, SPIE, 3356, 234
- Franceschini A., Silva L., Fasano G., Granato G.L., Bressan A., Arnouts S., Danese L., 1998, ApJ, 506, 600

- Franceschini A., Aussel H., Cesarsky C.J., Elbaz D., Fadda D., 2001, A&A, 378, 1
- Kauffmann G., Charlot S., White S.D.M., 1996, MNRAS, 283, 117
- Kauffmann G., Charlot S., 1998, MNRAS, 297, L23
- Kochanek C.S. et al., 2001, ApJ, 560, 566
- Larson R., 1975, MNRAS, 173, 671
- Longhetti M., Bressan A., Chiosi C., Rampazzo R., 2000, A&AS, 353, 917
- Lonsdale C. et al., 2004, ApJS, 154, L54
- Lotz J. Primack J., Madau P., 2004, AJ, 128, 163
- Madau P., Pozzetti L., 2000, MNRAS, 312, 9
- Mushotzky R.F. & Loewenstein M. 1997, ApJ, 481, L63
- Papovich C., Giavalisco M., Dickinson M., Conselice C.J., Ferguson H.C., 2003, ApJ, 598, 827
- Papovich C. et al., 2004, ApJS 154, 70
- Peng C.Y., Ho L.C., Impey C.D., Rix H.-W., 2002, ApJ, 124, 266
- Pignatelli E., Fasano G., Cassata P., 2005, A&A, submitted
- Ravindranath S. et al., 2004, ApJ, 604, 9L
- Rodighiero G., Franceschini A., Fasano G., 2001, MNRAS, 324, 491
- Rowan-Robinson M., 2001, ApJ, 549, 745
- Rowan-Robinson M. et al., 2005, AJ, 129, 1183
- Scalo J.M., 1986, Fundamentals of Cosmic Physics, 11, 1
- Sérsic J., 1968, *Atlas de Galaxias Australes Cordoba: Observatorio Astronomico*
- Silva L., Granato G.L., Bressan A., Danese, L., 1998, ApJ, 509, 103
- Somerville R.S., Primack J.R. 1999, MNRAS, 310, 1087
- Somerville R.S., Lee K., Ferguson H.C., Gardner J.P., Moustakas L.A., Giavalisco M., 2004, ApJ, 600, L135
- Surace J.A. et al., Data Release Version 1 Document, [http://data.spitzer.caltech.edu/popular/swire/20041027\\_enhanced\\_v1\\_EN1/documents/SWIRE\\_EN1\\_doc\\_20041027.pdf](http://data.spitzer.caltech.edu/popular/swire/20041027_enhanced_v1_EN1/documents/SWIRE_EN1_doc_20041027.pdf)
- Thomas D., Maraston C., Bender R. Mendes de Oliveira C., ApJ, 2005, 621, 673
- Windhorst R. A. et al., 2002, ApJS, 143, 113
- Wirth G.D. et al., 2004, AJ, 127, 3121
- White S.D.M., Rees M.J. 1978, MNRAS , 183, 341
- White S.D.M., Frenk C.S., 1991, ApJ, 379, 52
- Xu C.K., Lonsdale C.J., Shupe D.L., Franceschini A., Martin C., Schiminovich D., 2003, ApJ, 587, 90